Title	Non-local photo-polymerization kinetics including multiple termination mechanisms and dark reactions : part III. Primary radical generation and inhibition
Authors(s)	Gleeson, M. R.; Liu, Shui; Guo, Jinxin; Sheridan, John T.
Publication date	2010-09-01
Publication information	Journal of the Optical Society of America B, 27 (9): 1804-1812
Publisher	Optical Society of America
Link to online version	http://dx.doi.org/10.1364/JOSAB.27.001804
Item record/more information	http://hdl.handle.net/10197/3369
Publisher's statement	This paper was published in Journal of the Optical Society of America B and is made available as an electronic reprint with the permission of OSA. The paper can be found at the following URL on the OSA website: http://www.opticsinfobase.org/abstract.cfm?URI=josab-27-9-1804. Systematic or multiple reproduction or distribution to multiple locations via electronic or other means is prohibited and is subject to penalties under law.
Publisher's version (DOI)	10.1364/JOSAB.27.001804

Non-local photo-polymerization kinetics including multiple termination mechanisms and dark reactions: Part III. Primary radical generation and inhibition

Michael R. Gleeson,* Shui Liu, Jinxin Guo, and John T. Sheridan

School of Electrical, Electronic and Mechanical Engineering, Communication and Optoelectronic Research Centre, The SFI-Strategic Research Cluster in Solar Energy Conversion, College of Engineering, Mathematical and Physical Sciences, University College Dublin, Belfield, Dublin 4, Ireland
E-mail: john.sheridan@ucd.ie
**Corresponding author: michael.gleeson@ucd.ie*

Received April 13, 2010; revised July 5, 2010; accepted July 5, 2010;
posted July 6, 2010 (Doc. ID 126981); published August 13, 2010

Photopolymers are playing an ever more important role in diverse areas of research such as holographic data storage, hybrid photonic circuits, and solitary waves. In each of these applications, the production of primary radicals is the driving force of the polymerization processes. Therefore an understanding of the production, removal, and scavenging processes of free radicals in a photopolymer system is crucial in determining a material's response to a given exposure. One such scavenging process is inhibition. In this paper the non-local photo-polymerization driven diffusion model is extended to more accurately model the effects of (i) time varying primary radical production, (ii) the rate of removal of photosensitizer, and (iii) inhibition. The model is presented to specifically analyze the effects of inhibition, which occur most predominantly at the start of grating growth, and comparisons between theory and experiment are performed which quantify these effects.

OCIS codes: 090.7330, 090.2900, 050.1940, 160.5335, 160.5470, 300.1030.

1. INTRODUCTION

Photopolymer materials and the photochemical kinetics associated with them [1–10] have been studied extensively in both academia and industry due to the growing interest in applications involving photopolymers [11–18]. In order to maximize the potential of these materials for various applications, the necessity for a physically comprehensive theoretical model of the effects which occur during photo-polymerization is becoming ever more important [4,6–10,19–28]. Providing such a model will enable potential trends in a material's performance to be much more easily recognized and optimized [19,29]. Such models allow simulations of the effects of ratios of various key material parameters to be made, yielding indications of the most suitable material compositions in order to improve the material performance.

In this paper we extend some recently published results on the non-local photo-polymerization driven diffusion (NPDD) model [9,10]. The previous model provided a comprehensive theoretical representation of the processes, which occur during free radical photopolymerization. The physically realistic model enabled predictions to be made about a number of very different photopolymer materials [7,30]. In this paper, we present several extensions to the previous model in particular allowing for spatially and temporally varying primary radical generation. We then apply the improved model to analyze a number of effects observed to take place during holographic grating formation in an acrylamide/polyvinyl alcohol (AA/PVA) based photopolymer sensitized with a xanthene type dye, Erythrosin B [5,31–33], and compare experimental results and the predictions of the model with the aim of characterizing these effects.

This paper is structured as follows. In Section 2 we briefly examine the photochemical processes involved during holographic grating formation, reviewing some of the assumptions previously made. We then implement a more accurate representation of the initiation mechanisms occurring during exposure, thus increasing the physical validity of the model proposed. The governing set of truncated first-order coupled differential equations is generated. In Section 3, by applying suitable initial conditions, the differential equations are then solved numerically and simulations highlighting what we believe to be new predictions of the extended model are made. In Section 4 holographic grating refractive index modulation growth curves for various low exposure intensities are presented in order to emphasize the effects of inhibition, which are most clearly observed at the start of the grating formation. The model is then numerically fit to the experimental data in order to extract estimates of key material parameters. In Section 5 a brief conclusion is presented.

2. PHOTOCHEMICAL PROCESSES

A. Review of Kinetic Models

The photochemical processes, which are present during photopolymerization, are complex [9,21,22,31–33]; how-

ever an understanding of these processes is of utmost importance if a practical model is to be developed. In a recent review [29], many of the assumptions made in developing photochemical models of free radical photopolymerization were discussed [1–8,19–28]. A number of physical effects not included in the previous models were listed, which indicated a lack of physicality under certain exposure conditions. Following the appearance of this review, a series of papers were published [9,10] which addressed many of these issues and provided a model containing a consistent set of chemical reaction equations to take into account many of these effects. These effects included:

(i) removal of the steady state approximation for macroradical concentration,
(ii) inclusion of spatially and temporally non-local polymer chain growth,
(iii) inclusion of time varying photon absorption,
(iv) simultaneously including the effects of both primary, i.e., $R^{\bullet}$-$M^{\bullet}$, and bimolecular, i.e., $M^{\bullet}$-$M^{\bullet}$, terminations,
(v) inclusion of the changes in the polymerization kinetic constants caused by increased viscosity, and finally
(vi) inclusion of polymerization inhibiting effects.

The resulting NPDD model was then experimentally verified by applying it to study (a) normalized transmission curves and (b) growth curves of the refractive index modulation for both short and continuous holographic exposures, in two significantly different free radical photopolymer materials [5,7,30]. The quality of the fits obtained for both photopolymer materials indicated the versatility and applicability of the model.

In the past number of years, extensive work has been presented in the literature to describe the time varying absorption effects, which occur in photopolymer materials during exposure [31–36]. In all cases the aim has been to improve the understanding of the photo-kinetics occurring in these materials, and critically to enable accurate predictions of the generation of primary radicals. A model of photosensitizer behavior proposed by Carretero *et al.* [35] has recently been extended to account for (i) photon absorption, (ii) regeneration or recovery of the absorptive photosensitizer, and (iii) photosensitizer bleaching [31–34]. Using this model an expression for the time varying absorbed intensity, $I_a(t)$ (Einstein/cm^3 s), was derived and the values of key material parameters were estimated using nonlinear fits of the dye model to experimentally obtained transmission curves. The processes of primary radical generation were described in these papers using the expression [37]

$$R_i = 2\Phi I_a(t), \tag{1}$$

where R_i is the rate of generation of primary radicals and Φ is the number of primary radicals initiated per photon absorbed. The factor of 2 indicates that radicals are created in pairs [9,10,31–37].

In this paper, we extend the NPDD model in [9,10] by more accurately representing the temporal and spatial variation of photosensitizer concentration and the associated temporal and spatial generation and removal of primary radicals. As a result the number of approximations made in modeling the photo-initiation kinetics is significantly reduced. Thus a more physically accurate representation of the photo-polymerization kinetics is produced. Crucially, the proposed model enables a more physically realistic and accurate analysis of the process of inhibition.

B. Reaction Mechanisms

The kinetic model presented in this analysis is based on the following four reaction processes [1–5,9,37]:

I. Initiation

$$I \xrightarrow{h\nu} R^{\bullet}, \tag{2a}$$

$$R^{\bullet} + M \xrightarrow{k_i} M_1^{\bullet} = \text{chain initiator}. \tag{2b}$$

II. Propagation

$$M_n^{\bullet} + M \xrightarrow{k_p} M_{n+1}^{\bullet} = \text{growing polymer chain}. \tag{3}$$

III. Termination

$$M_n^{\bullet} + M_m^{\bullet} \xrightarrow{k_{tc}} M_{n+m} = \text{dead polymer}, \tag{4a}$$

$$M_n^{\bullet} + M_m^{\bullet} \xrightarrow{k_{td}} M_n + M_m = \text{dead polymer}, \tag{4b}$$

$$M_n^{\bullet} + R^{\bullet} \xrightarrow{k_{tp}} M_n R = \text{dead polymer}. \tag{4c}$$

IV. Inhibition [37–39]

$$D^* + Z \xrightarrow{k_{z,\mathrm{Dye}^*}} \text{leuco dye} + Z^*, \tag{5a}$$

$$R^{\bullet} + Z \xrightarrow{k_{z,R^{\bullet}}} (R + Z^{\bullet} \text{ and/or } RZ^{\bullet}) = \text{scavenged radical}, \tag{5b}$$

$$M_n^{\bullet} + Z \xrightarrow{k_{z,M^{\bullet}}} (M_n + Z^{\bullet} \text{ and/or } M_n Z^{\bullet}) = \text{dead polymer}. \tag{5c}$$

In the above set of chemical equations; I is the initiator concentration; $h\nu$ indicates the energy absorbed from a photon; M is the monomer concentration; Z is the inhibitor concentration; M_n, M_m, M_{n+m}, M_nR, and $M_nZ^{\bullet}$ represent polymer species with no active propagating tip, i.e., *dead polymer*. D^* is the concentration of excited photosensitizer and Z^* is the concentration of singlet oxygen [33,34,37–39]. The term *dead polymer* signifies the cessation of the growth of a propagating macroradical of n monomer repeat units [37], while the term *scavenged radical* signifies the removal of a primary radical [37–39]. k_p, k_{tc}, k_{td}, $k_{z,M^{\bullet}}$, k_{z,Dye^*}, and $k_{z,R^{\bullet}}$ (cm^3 mol^{-1} s^{-1}) are the rate constants of propagation, termination by combination, termination by disproportionation, inhibition of macroradicals, inhibition of excited dye molecules and inhibition of primary radicals, respectively.

C. Primary Radical Production

As can be seen in Eqs. (2), the initiation process involves two steps: The *first step* is the production of free radicals by homolytic dissociation of the initiator to yield an initiator (primary) radical, $R^\bullet$, i.e., Eq. (2a). The *second step* is the chain initiation, i.e., Eq. (2b), in which the primary radicals produced due to the absorption of photons react with the monomer to produce the chain initiating species $M_1^\bullet$ [1–4,37]. The kinetic rate constant for this step is k_i ($\text{cm}^3\ \text{mol}^{-1}\ \text{s}^{-1}$), i.e., the chain initiation kinetic constant. As stated the main extensions to the previous model [9,10] involve improvements to the modeling of the temporal and spatial variations in primary radical production. Therefore, the main focus of this subsection will be the first step of the initiation mechanism, which is presented in Eq. (2a).

In order to do this, we assume that the following photochemical reactions take place upon illumination of a photopolymer layer sensitized with a xanthene or thiazine type photosensitizer [5] of appropriate wavelength. These are as follows:

$$D + h\upsilon \xrightarrow{ka} D^*, \tag{6a}$$

$$D^* + Z \xrightarrow{kz,D} \text{leuco dye}, \tag{6b}$$

$$D^* \xrightarrow{kr} D, \tag{6c}$$

$$D^* + CI \xrightarrow{kd} R^\bullet + H^+ + D^{\bullet -} \rightarrow R^\bullet + HD^\bullet, \tag{6d}$$

$$CI + HD^\bullet \xrightarrow{kb} H_2D + CI_{\text{int}}. \tag{6e}$$

In these equations D represents the concentration of the photosensitizer (dye); $h\nu$ represents the photon energy incident on the material; D^* is the excited state of the dye, CI is the co-initiator; $R^\bullet$ represents the primary radical concentration; Z is the inhibitor; $HD^\bullet$ represents a radicalized dye, which has abstracted a hydrogen from the co-initiator; and H_2D is the transparent di-hydro form of the dye. CI_{int} is an intermediate form of the co-initiator, which is no longer available for reaction.

k_a (s^{-1}) is the rate of production of the excited state photosensitizer, k_r (s^{-1}) is the rate of recovery or regeneration of the photo-absorber, k_d ($\text{cm}^3\ \text{mol}^{-1}\ \text{s}^{-1}$) is the rate of dissociation of the initiator, and $k_{z,D}$ ($\text{cm}^3\ \text{mol}^{-1}\ \text{s}^{-1}$) is the inhibition rate constant associated with the reaction with excited dye molecules. We note that previous models of the photo-initiation kinetics have not included all the reactions specified in Eqs. (6).

In order to use the proposed rate equations in the next subsection, it is first necessary to convert the exposure intensity I_0 (mW/cm^2) to the appropriate units (Einsteins/cm^3 s). This can be done using $I_0' = (T_{sf} B I_0/d) \times (\lambda/N_a hc)$, where λ (nm) is the wavelength of the incident light, N_a (mol^{-1}) is Avogadro's constant, c (m/s) is the speed of light, and h (J s) is Plank's constant. $B = 1 - e^{-\varepsilon D_0 d}$ is the absorptive fraction which determines a material layer's initial absorptive capacity and is a function of the dye's initial concentration D_0 (mol/cm^3), T_{sf} is a fraction associated with the light lost by Fresnel and scattering losses [8,31–35], molar absorptivity ε (cm^2/mol), and material layer thickness d (cm).

The rate of production of the excited state photosensitizer, appearing in Eq. (6a), is then represented by $k_a = \phi \varepsilon d I_0'$ (s^{-1}), where ϕ (mol/Einstein) is the quantum efficiency of the reaction [37]. Therefore, if the photosensitizer's initial concentration, molar absorptivity, quantum efficiency, and layer thickness are known, the rate of generation of the excited state photosensitizer, D^*, can be determined for a given exposure intensity.

D. Model Development

In the case of holographic illumination, there is a spatial distribution of irradiance, which in our case is typically cosinusoidal. In this case the incident intensity is represented as $I(x,t) = I_0'[1 + V\cos(Kx)]$, where V is the fringe visibility and $K = 2\pi/\Lambda$, where Λ is the grating period. The mechanisms, which are presented in Eqs. (6), can then be represented by a set of coupled differential equations. The combination of these equations is equivalent to the previous representation of primary radical production in time and space, which is presented in Eq. (1). Combining these equations with those previously presented in [9,10], describing the mechanisms of initiation, propagation, termination, and inhibition, yields the following set of first-order coupled differential equations governing the photosensitizer:

$$\frac{dD(x,t)}{dt} = -k_a D(x,t) + k_r D^*(x,t), \tag{7}$$

$$\frac{dD^*(x,t)}{dt} = k_a D(x,t) - k_r D^*(x,t) - k_d D^*(x,t) CI(x,t) - k_{z,D} D^*(x,t) Z(x,t), \tag{8}$$

$$\frac{dCI(x,t)}{dt} = -k_d D^*(x,t) CI(x,t) - k_b HD^\bullet(x,t) CI(x,t), \tag{9}$$

$$\frac{dHD^\bullet(x,t)}{dt} = k_d D^*(x,t) CI(x,t) - k_b HD^\bullet(x,t) CI(x,t). \tag{10}$$

As in the previous analysis [9,10], it is assumed that the effect of inhibition during exposure is due solely to the initially dissolved oxygen present within the photopolymer layer. The non-uniform recording irradiance causes concentration gradients of oxygen as it is consumed in inhibitory reactions. This then results in the diffusion of oxygen from the dark non-illuminated regions to the bright illuminated regions. As oxygen molecules are small compared to the other material components which constitute the photopolymer layer, it can be assumed that the oxygen is relatively free to diffuse rapidly, resulting in a one-dimensional standard diffusion equation for the concentration of inhibitor,

$$\frac{dZ(x,t)}{dt} = \frac{d}{dx}\left[D_z \frac{dZ(x,t)}{dx}\right] - k_{z,D} D^*(x,t) Z(x,t) - k_{z,R^\bullet} Z(x,t) R^\bullet(x,t) - k_{z,M^\bullet} Z(x,t) M^\bullet(x,t), \quad (11)$$

where Z is the instantaneous inhibiting oxygen concentration and D_z is the diffusion constant of oxygen in the dry material layer, which in this analysis will be assumed to be time and space independent. This assumption is reasonable, as this fast rate of diffusion of the small oxygen molecule will not be significantly affected by any small changes in material viscosity. The inhibition rate constants, $k_{z,R^\bullet}$ and $k_{z,M^\bullet}$, will in general have different values (of reactivity) due to the differences in the relative molecular size [37]. However in this analysis, for the sake of simplicity, we assume $k_z = k_{z,R^\bullet} = k_{z,M^\bullet}$. Furthermore it is expected that the reactivity of oxygen with the excited state form of the photosensitizer will be much lower, i.e., $k_{z,D} \ll k_z$, and therefore we assume that it can be neglected in this analysis [33]. As before [9,10], it is assumed that the inhibition rate constant can be expressed as

$$k_z = k_{z,0} \exp(-E_z/RT), \quad (12)$$

where in this equation $k_{z,0}$ ($\mathrm{cm^3\ mol^{-1}\ s^{-1}}$) is the Arrhenius pre-exponential factor, $E_z = 18.23 \times 10^3$ J $\mathrm{mol^{-1}}$ is the activation energy of oxygen (i.e., the energy that must be overcome in order for oxygen to react with the given species), $R = 8.31$ J $\mathrm{K^{-1}\ mol^{-1}}$ is the universal gas constant, and T (K) is the local temperature [37].

The equation governing the concentration of primary radicals, including the new term for primary radical generation, is given by

$$\frac{dR^\bullet(x,t)}{dt} = k_d D^*(x,t) CI(x,t) - k_i R^\bullet(x,t) u(x,t) - k_{tp} R^\bullet(x,t) M^\bullet(x,t) - k_z R^\bullet(x,t) Z(x,t), \quad (13)$$

where $u(x,t)$ is the free-monomer concentration (denoted earlier in the chemical reactions by M). This equation states that the rate of change of primary radical concentration is proportional to the concentration of primary radicals generated by photon absorption, minus the amounts removed by the (a) initiation of macroradicals, (b) primary termination with growing polymer chains, and (c) inhibition by oxygen.

Including both types of termination mechanism (primary and bimolecular) and the effects of inhibition, the equation governing macroradical concentration is then

$$\frac{dM^\bullet(x,t)}{dt} = k_i R^\bullet(x,t) u(x,t) - k_t [M^\bullet(x,t)]^2 - k_{tp} R^\bullet(x,t) M^\bullet(x,t) - k_z Z(x,t) M^\bullet(x,t), \quad (14)$$

where the squared term $[M^\bullet(x,t)]^2$ represents the effects of bimolecular termination. The generation term in this equation previously appears as the removal term due to macroradical initiation in Eq. (13).

The non-uniform irradiance creates monomer concentration gradients, and as a result monomer diffuses from the dark regions to the monomer depleted exposed regions. This results in a spatial polymer concentration distribution, which provides the modulation of the refractive index in the material, i.e., the holographic grating. We represent the monomer concentration using the following one-dimensional diffusion equation:

$$\frac{du(x,t)}{dt} = \frac{d}{dx}\left[D_m(x,t) \frac{du(x,t)}{dx}\right] - k_i R^\bullet(x,t) u(x,t) - \int_{-\infty}^{\infty} k_p M^\bullet(x',t) u(x',t) G(x,x')\,dx', \quad (15)$$

where $D_m(x,t)$ represents the monomer diffusion constant. $G(x,x')$ is the non-local material spatial response function given by [25]

$$G(x,x') = \frac{1}{\sqrt{2\pi\sigma}} \exp\left[\frac{-(x-x')^2}{2\sigma}\right], \quad (16)$$

where σ is the constant non-local response parameter normalized with respect to the grating period Λ. This non-local spatial response function represents the effect of initiation at location x' on the amount of monomer polymerized at location x.

The equation governing the polymer concentration N is

$$\frac{dN(x,t)}{dt} = \int_{-\infty}^{\infty} k_p M^\bullet(x',t) u(x',t) G(x,x')\,dx' - \frac{d}{dx}\left[D_N(x,t) \frac{dN(x,t)}{dx}\right], \quad (17)$$

where $D_N(x,t)$ represents the polymer diffusion constant. As with the monomer above in Eq. (15), the non-uniform irradiance creates a polymer concentration distribution. If the polymer chains are not cross-linked, they will tend to diffuse out of the exposed regions in order to reduce the polymer gradient [8,40]. If this takes place it will result in a decay of the grating strength with time. However, in this paper we assume that there is sufficient cross-linking so that $D_N(x,t) = 0$, i.e., very stable gratings are recorded. We also note that this is supported by results reported in the literature [8], using the same material composition.

Since all the above equations presented in Eqs. (7)–(11), (13)–(15), and (17) depend on the spatial distribution of the exposing intensity, they will all be periodic even functions of x and can therefore be written as Fourier series, i.e., $X(x,t) = \Sigma_{j=0}^{\infty} X_j(t) \cos(jKx)$, where X represents the species concentrations D, D^*, CI, $HD^\bullet$, $R^\bullet$, $M^\bullet$, u, N, and Z. A set of first-order coupled differential equations can then be obtained in the same manner presented in [9,10], by gathering the coefficients of the various cosinusoidal spatial contributions and writing the equations in terms of these time varying spatial harmonic amplitudes. These coupled equations can then be solved using the following initial conditions:

$$Z_0(t=0) = Z_0, \quad D_0(t=0) = D_0, \quad CI_0(t=0) = CI_0, \quad u_0(t=0) = U_0,$$

$$D^{*}_{n\geq 0}(t=0) = HD^{\bullet}_{n\geq 0}(t=0) = R^{\bullet}_{n\geq 0}(t=0) = M^{\bullet}_{n\geq 0}(t=0) = N_{n\geq 0}(t=0) = 0,$$

$$D_{n>0}(t=0) = CI_{n>0}(t=0) = Z_{n>0}(t=0) = 0. \quad (18)$$

The equations governing the monomer and polymer harmonic amplitudes include the non-local response parameter σ, the effects of which appear in the coupled differential equations in $S_i = \exp(-i^2K^2\sigma/2)$ [25].

3. MODEL SIMULATIONS

Before applying the theoretical model presented in the previous section to fit experimental data we wish to examine its general behavior. In all theoretical simulations presented here, it is assumed that time varying viscosity effects are negligible and that $D_m(x,t) = D_{m0} = 8.0 \times 10^{-11}$ cm^2/s [22]. All kinetic parameter values are assigned values (typical for the AA/PVA photopolymer material examined here) [5,7,9,10].

12 spatial concentration harmonics are retained in the simulations, solved using the initial conditions presented in Eq. (18) with $U_0 = 2.83 \times 10^{-3}$ mol/cm^3, $D_0 = 1.22 \times 10^{-6}$ mol/cm^3, $CI_0 = 3.18 \times 10^{-3}$ mol/cm^3, and $Z_0 = 1 \times 10^{-8}$ mol/cm^3. Assuming typical recording conditions for an unslanted transmission type volume holographic grating, $\Lambda = 700$ nm and fringe visibility $V = 1$, simulations of the temporal and spatial variations in the photosensitizer concentration $D(x,t)$ are generated and presented in Fig. 1(a). The typical rate constants used were $k_p = k_i = 2.65 \times 10^7$ cm^3/mol s, $k_t = 6 \times 10^9$ cm^3/mol s, $k_{tp} = k_t \times 10$, $k_d = k_b = 1.6 \times 10^3$ cm^3/mol s, $k_z = 3 \times 10^{12}$ cm^3/mol s, and $k_r = 1.22 \times 10^{-3}$ s^{-1} [9,10,31–34]. For an exposure intensity of $I_0 = 1$ mW/cm^2 and $\lambda = 532$ nm, the absorption parameters estimated from fits to normalized transmission curves for a material layer of thickness $d = 100$ μm are $\varepsilon = 1.4 \times 10^8$ cm^2/mol, $\phi = 0.066$ mol/Einstein, and $T_{sf} = 0.76$, with $N_a = 6.02 \times 10^{23}$ mol^{-1}, $c = 3 \times 10^8$ ms^{-1}, and $h = 6.62 \times 10^{-34}$ J s [31–34]. The oxygen diffusion coefficient was assumed to be $D_z = 1.0 \times 10^{-8}$ cm^2/s [41]. The parameter S_1, which quantifies the extent of the non-locality in the first harmonic coupled differential equation, was chosen to have a value of $S_1 = 0.94$. This corresponds to a non-local response length of $\sqrt{\sigma'} = 54$ nm [8].

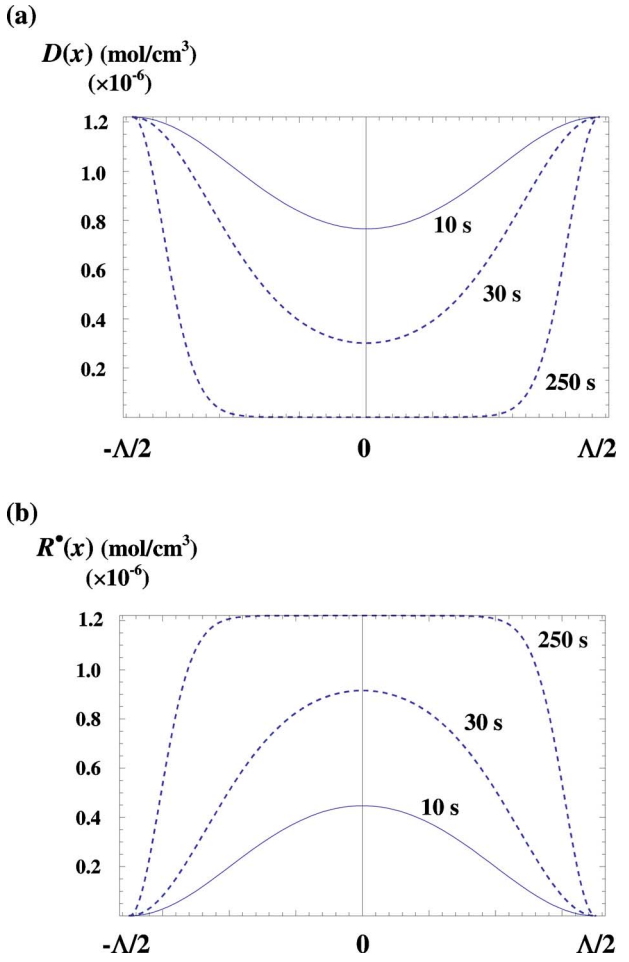

Fig. 1. (Color online) Simulation of the spatial variation of (a) the ground state photosensitizer concentration and (b) the generation of primary radicals, for an exposure intensity of $I_0 = 1$ mW/cm^2, at $\Lambda = 700$ nm, for various exposure times: $t_{exp} = 10$ s (solid line), $t_{exp} = 30$ s (dashed line), $t_{exp} = 250$ s (longer dashed line).

As can be observed from Fig. 1(a), the sinusoidal exposing interference pattern causes a rapid consumption of the ground state dye in the bright regions. As the exposure time increases the sinusoidal variation of the dye concentration is distorted and the width of the non-illuminated dark bands narrows. This loss in sinusoidal fidelity results in a spatial production of primary radicals, as shown in Fig. 1(b), which deviates significantly from the sinusoidal primary radical generation term presented in Eq. (1). Subsequently, this yields a nonlinear material response, as the number of polymer chains initiated (discussed in Section 2) is not simply generated in direct proportion to the exposing interference pattern. This is an important prediction of the model, which agrees well with experimental observation.

Using the same parameter values used to generate Fig. 1, Fig. 2 shows a simulation of the amplitudes of the first two concentration harmonics of the monomer, u_0 and u_1, and the corresponding polymer variations, N_0 and N_1. The presence of a "deadband" or inhibition period t_i can be observed at the early stages of exposure as a result of the inhibitory reactions. This behavior is consistent with the reaction mechanisms discussed in Section 2, where the primary radicals and macroradicals are scavenged by oxygen, which is initially dissolved in the photopolymer layer.

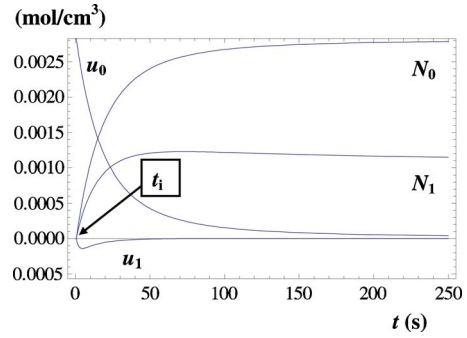

Fig. 2. (Color online) Simulations of the variation of the first two concentration harmonics of monomer and polymer using the theoretical model.

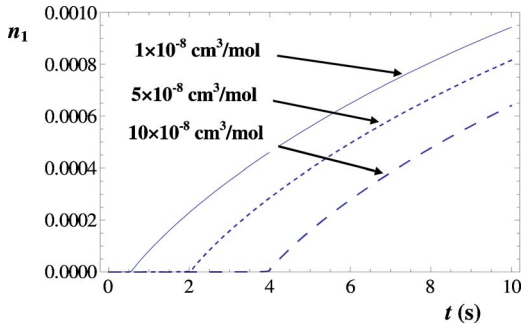

Fig. 3. (Color online) Simulations of the refractive index modulation with time, for various values of dissolved oxygen concentration. $Z_0=1\times10^{-7}$ mol/cm^3 (long-dashed line), $Z_0=5\times10^{-8}$ mol/cm^3 (short-dashed line), and $Z_0=1\times10^{-8}$ mol/cm^3 (solid line).

Figure 3, shows the corresponding predicted refractive index modulation growth curves for varying values of the concentration of initially dissolved oxygen, Z_0 (mol/cm^3), 1×10^{-8} mol/cm^3 (solid line), 5×10^{-8} mol/cm^3 (short dashed line), and 1×10^{-7} mol/cm^3 (long dashed line). As the concentration of the inhibitor is increased, the inhibition time t_i increases as expected, i.e., more inhibitor increases the deadband associated with the scavenging of the primary radicals and macroradicals.

4. EXPERIMENTAL ANALYSIS

A set of unslanted transmission type volume holographic gratings were recorded at a spatial frequency of 1428 lines/mm in an uncoverplated [39] AA/PVA based photopolymer sensitized with Erythrosin B [5,7,9,10], with a recording wavelength of $\lambda_r=532$ nm at a range of low exposure intensities $I_{01}=0.2$ mW/cm^2, $I_{02}=0.1$ mW/cm^2, and $I_{03}=0.05$ mW/cm^2. These low exposure intensities were chosen in order to emphasize and permit a detailed study of the effects of inhibition, which are most evident at the start of grating growth. The growth of the grating was monitored using a probe wavelength of $\lambda_p=633$ nm, and the resulting first-order diffracted intensity $I_D(t)$ was measured and then processed to correct for Fresnel reflection losses. The refractive index modulation n_1 was then extracted from the measured diffraction efficiency, $\eta(t)=I_D(t)/I_0'$, using first-order electromagnetic coupled wave theory [42],

$$\eta(t)=\sin^2\left[\frac{\pi d n_1(t)}{\lambda_p\cos\theta_{\text{in}}}\right], \tag{19}$$

where d is the thickness of the material layer, λ_p is the wavelength of the probe/replay laser, and θ_{in} is the angle inside the layer at which the Bragg condition is satisfied [42].

In order to accurately apply the model it is first necessary to obtain several parameters which govern the photopolymer's behavior. These parameters include the volume fractions and refractive indices of each of the material components. These values have been previously reported for the AA/PVA photopolymer material under examination here [8–10,27]. Given these values the Lorentz–Lorenz relation is used to determine the temporal evolution of the refractive index modulation,

$$n_1(t)=\frac{(n_{\text{dark}}^2+2)^2}{6n_{\text{dark}}}\left[\phi_1^{(m)}(t)\left(\frac{n_m^2-1}{n_m^2+2}-\frac{n_b^2-1}{n_b^2+2}\right)+\phi_1^{(p)}(t)\times\left(\frac{n_p^2-1}{n_p^2+2}-\frac{n_b^2-1}{n_b^2+2}\right)\right]. \tag{20}$$

In implementing this equation it is assumed that the total volume fraction of the material is conserved, i.e., $\phi^{(m)}(t)+\phi^{(p)}(t)+\phi^{(b)}(t)=1$, where $\phi^{(m)}(t)$, $\phi^{(p)}(t)$, $\phi^{(b)}(t)$ are the volume fractions of monomer, polymer, and background, respectively [9,10,23,27]. For low exposure intensities such as those examined in this paper, bimolecular termination is the dominant termination mechanism and therefore it is assumed that all monomer-consuming reactions result in the production of polymers. Furthermore it is assumed that material shrinkage effects are negligible. n_m, n_p, and n_b are the refractive indices of the monomer, polymer, and background and n_{dark} is the refractive index of the photopolymer layer before photo-polymerization measured at the probing wavelength [8–10,27]. $\phi_1^{(m)}(t)$ and $\phi_1^{(p)}(t)$ are the time varying first harmonic volume fraction components of monomer and polymer, respectively. Values for these are generated directly based on the concentrations predicted by the coupled differential equations in Section 2.

The following values are known *a priori* from previous examinations: $n_m=1.4719$, $n_b=1.4957$, $n_p=1.52$ and $n_{\text{dark}}=1.4948$ [8–10,27], $d=100$ μm, $\varepsilon=1.4\times10^8$ cm^2/mol, $\phi=0.066$, $T_{\text{sf}}=0.76$, $N_a=6.02\times10^{23}$ mol^{-1}, $c=3\times10^8$ m s^{-1}, and $h=6.62\times10^{-34}$ J s [9,10,31–34]. As noted $S_1=0.94$. Furthermore $U_0=2.83\times10^{-3}$ mol/cm^3, $D_0=1.22\times10^{-6}$ mol/cm^3, $CI_0=3.18\times10^{-3}$ mol/cm^3, and $Z_0=1\times10^{-8}$ mol/cm^3 [5,7–10].

A least-squares fitting algorithm is used in which the mean square error (MSE) cost function, which quantifies the difference between the theoretical prediction and the experimental growth curve data, was iteratively minimized, so as to obtain a best fit as a function of the unknown material parameters. These unknown parameters were restricted to sensible search ranges [3,4,9,10,22,37].

Comparing the experimental results with the theoretical prediction, it became clear that, when using the model as presented, the trend of increased inhibition times t_i for reduced exposure intensities did not satisfactorily replicate the experimental behavior observed. In order to achieve good fits to the experimental data, it was found necessary to assume a larger initial concentration of dissolved oxygen available in the photopolymer layer, Z_0, and that this concentration increased as the recording intensities were reduced. The variation between the experimentally observed inhibition period and theoretical prediction was as much as 8 s for the lowest recording intensity examined in this paper for unsealed layers. This divergence between experiment and prediction suggests that the model is incomplete and that in order to mimic the physically observed behavior amendments to the model are necessary.

In a previous paper [39] it was found that, by coverplating or sealing the photopolymer layer with glass slides, the inhibition times observed during exposure were significantly reduced compared with the corresponding un-

coverplated or unsealed layers. These effects were attributed to the removal or reduction of oxygen diffusing in from the surrounding environment, which was replacing or replenishing the oxygen consumed during exposure. It must be noted at this point that the experimental data examined so far were for uncoverplated photopolymer layers, which were subject to such external oxygen diffusion.

In order to represent this process in the model, an additive term representing the replenishing of inhibiting oxygen from the outside surrounding air, into the material layer, was included. Therefore, Eq. (11) must be revised and becomes

$$\frac{dZ(x,t)}{dt} = \frac{d}{dx}\left[D_z \frac{dZ(x,t)}{dx}\right] - k_{z,D}D^*(x,t)Z(x,t) - k_{z,R^\bullet}Z(x,t)R^\bullet(x,t) - k_{z,M^\bullet}Z(x,t)M^\bullet(x,t) + \tau_z[Z_0 - Z(x,t)], \quad (21)$$

where τ_z represents the rate of replenishing of oxygen into the material layer. We note that it is assumed that the oxygen concentration can never be larger than the original dissolved oxygen concentration Z_0 (mol/cm^3) and that this additive term is assumed to be spatially constant.

In order to illustrate these effects Fig. 4 shows a simulation of the behavior of the oxygen concentration with varying values of the replenishing constant τ_z for an exposure intensity of $I_0=0.04$ mW/cm^2 and exposure time of $t_{exp}=30$ s. As can be observed, an increase in τ_z results in (i) an increase in the inhibition period and (ii) an increase in the rate at which oxygen returns to its original dissolved oxygen concentration, post-exposure.

Solving Eq. (21) under the same initial conditions, the model is fit to the experimental growth curves recorded in uncoverplated layers, yielding much more consistent fits to the data. Figure 5 shows a subset of this data with the corresponding fits obtained using the model. Some of the parameter values obtained from the fits to a variety of

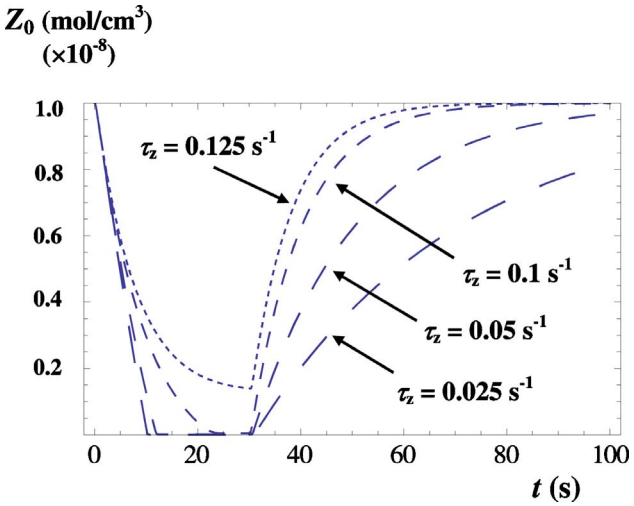

Fig. 4. (Color online) Simulation of the behavior of the oxygen concentration with varying values of τ_z, for an exposure time of $t_{exp}=30$ s and exposure intensity of $I_0=0.04$ mW/cm^2. $\tau_z=0.125$ s^{-1} (shorter-dashed line), $\tau_z=0.1$ s^{-1} (short-dashed line), $\tau_z=0.05$ s^{-1} (long-dashed line), $\tau_z=0.025$ s^{-1} (longer-dashed line).

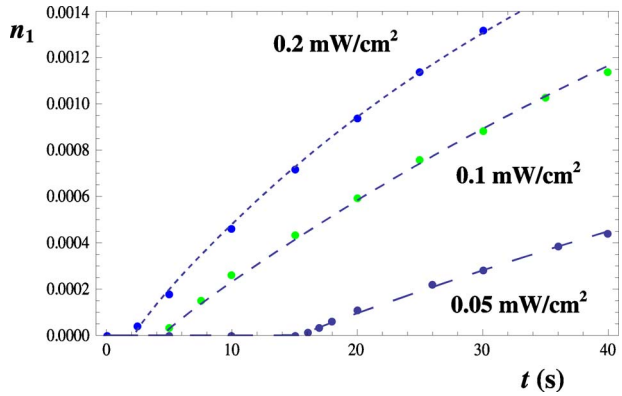

Fig. 5. (Color online) Experimentally obtained refractive index modulation growth curves recorded in uncoverplated AA/PVA photopolymer material layers at a spatial frequency of 1428 lines/mm for three different exposing intensities: $I_{01}=0.2$ mW/cm^2 (short-dashed line), $I_{02}=0.1$ mW/cm^2 (dashed line), and $I_{03}=0.05$ mW/cm^2 (long-dashed line) with corresponding fits achieved with the theoretical model.

exposure intensities are $k_d=1.6\times10^3$ cm^3/mol s, $k_r=1.2\times10^{-3}$ s^{-1}, $k_z=3.0\times10^{12}$ cm^3/mol s, and $D_z=1\times10^{-8}$ cm^2/s. In all cases it was assumed in all fits that $k_{tp}=10\times k_t$ cm^3/mol s and $k_i=k_p$ cm^3/mol s. The most significant values extracted from the fits are presented in Table 1 along with the parameter search ranges, which were used to obtain a best fit. These search ranges are typical of the valued presented in the literature for similar photopolymer materials [3,4,37]. The best fit MSE values achieved are also included to indicate the quality of the fits.

As can be observed from Fig. 5, the fit quality is very good and the model predicts the observed trend, i.e., that a reduction in the exposure intensity causes an increase in the inhibition period due to (i) the initially dissolved oxygen and (ii) oxygen diffusion into the material from the surrounding air. It can also be seen that there is a reduction in the propagation and termination rates with increasing exposure intensities. This is most likely due to the increased viscosity effects, which occur due to the increased conversion of monomer to polymer [2–4,9]. This is consistent with the results obtained from the previous model [10]. It must also be noted at this point that the estimates obtained for the rates of propagation and termination are slightly higher than those previously reported [10]. This is as a result of a more physically accurate description of the primary radical generation introduced by the model development. The estimated values extracted still remain well within the accepted ranges presented in the literature for similar photopolymer materials [3,4,37].

In order to verify the necessity for the inclusion of the additive oxygen replenishing term in Eq. (21), several growth curves of the refractive index modulation were recorded in coverplated layers. These growth curves were recorded under the same conditions as the uncoverplated layers presented in Fig. 5. Figure 6 shows experimental growth curves recorded at an exposure intensity of $I_0=0.05$ mW/cm^2, in corresponding coverplated and uncoverplated layers. The subsequent fits to the experimental data, which were achieved using the revised model, are represented as short (coverplated) and long (uncover-

Table 1. Parameters Extracted from Fits to Experimentally Obtained Growth Curves of Refractive Index Modulation in Uncoverplated Photopolymer Layers

I_0 (mW/cm^2)	t_i (s)	k_p ($\times 10^7$) (cm^3/mol s)	k_t ($\times 10^9$) (cm^3/mol s)	D_{m0} ($\times 10^{-11}$) (cm^2/s)	τ_z (s^{-1})	MSE ($\times 10^{-11}$)
0.20	2.50	2.42	5.0	8.0	0.075	1.05
0.10	4.50	2.52	7.0	9.0	0.080	2.86
0.05	16.00	3.00	7.0	10.0	0.115	1.88
Search range	—	0.1–5.0	0.1–9.0	1.0–12.0	—	—

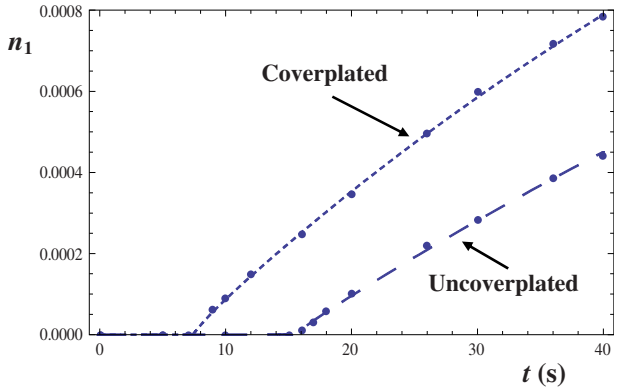

Fig. 6. (Color online) Experimentally obtained refractive index modulation growth curves recorded in both coverplated (short-dashed line) and uncoverplated (long-dashed line) AA/PVA photopolymer material layers at a spatial frequency of 1428 lines/mm for a recording intensity of $I_0 = 0.05$ mW/cm^2 with corresponding fits achieved with the theoretical model.

plated) dashed lines. As can be observed from the figure there is a significant reduction in the inhibition period, from $t_i = 16$ s (uncoverplated) to $t_i = 9$ s (coverplated). As stated above, this is attributed to a reduction in the amount of oxygen available through diffusion into the layer from the surrounding air. The estimated parameters extracted from these fits are presented in Table 2. The values determined for the replenishing rate τ_z are consistent with what is experimental observed.

5. CONCLUSIONS

In this paper, further developments of the non-local photo-polymerization driven diffusion (NPDD) model [9,10] are presented. For the first time, the spatial and temporal variations in primary radical generation are included. These extensions provide a more physically comprehensive theoretical representation of the processes, which occur during free radical photo-polymerization.

A clearer more physical representation of the reactions, which take place during the photo-initiation stages, was provided, including the spatial and temporal consumption and regeneration of the photosensitizer and the reactions between the excited dye molecules and the co-initiator. Simulations are presented, which highlight the loss of sinusoidal fidelity of the primary radical generation distribution. This behavior deviates from that which was previously assumed in the literature. Subsequently, this change in the spatial generation of primary radicals has a substantial effect on the distribution of the polymer chains formed and, hence, on the resulting refractive index modulation recorded.

The model was then further extended to incorporate the effect of oxygen diffusion from outside the material layer by including a rate of oxygen replenishment. This allowed accurate modeling of the inhibition effects, which dominate the start of grating growth. The results obtained are consistent with the results of previous studies where coverplating techniques were used. Future work will include an experimental examination of the effects of high exposure intensities on the behavior of the primary radical generation and the complete inclusion of the modeling of time varying viscosity effects within the material.

ACKNOWLEDGMENTS

We acknowledge the support of Enterprise Ireland and Science Foundation Ireland through the Research Innovation and Proof of Concept Funds, and the Basic Research and Research Frontiers Programmes. We acknowledge the support of the Irish Research Council for Science, Engineering and Technology.

Table 2. Parameters Extracted from Fits to Experimentally Obtained Growth Curves Recorded at $I_0 = 0.05$ mW/cm^2 for Coverplated and Uncoverplated Polymer Layers

	t_i (s)	k_p ($\times 10^7$) (cm^3/mol s)	k_t ($\times 10^9$) (cm^3/mol s)	D_{m0} ($\times 10^{-11}$) (cm^2/s)	τ_z (s^{-1})	MSE ($\times 10^{-11}$)
Coverplated	9.0	2.9	7.0	10.0	0.000	2.26
Uncoverplated	16.0	3.0	7.0	10.0	0.115	1.88
Search range	—	0.1–5.0	0.1–9.0	1.0–12.0	—	—

REFERENCES

1. C. H. Bamford, A. D. Jenkins, and R. Johnston, "Termination by primary radicals in vinyl polymerization," Trans. Faraday Soc. **55**, 1451–1460 (1959).
2. C. Decker, B. Elzaouk, and D. Decker, "Kinetic study of ultrafast photopolymerizations reactions," J. Macromol. Sci., Pure Appl. Chem. **33**, 173–190 (1996).
3. M. D. Goodner, H. R. Lee, and C. N. Bowman, "Method for determining the kinetic parameters in diffusion-controlled free-radical homopolymerizations," Ind. Eng. Chem. Res. **36**, 1247–1252 (1997).
4. M. D. Goodner and C. N. Bowman, "Modeling primary radical termination and its effects on autoacceleration in photopolymerization kinetics," Macromolecules **32**, 6552–6559 (1999).
5. J. R. Lawrence, F. T. O'Neill, and J. T. Sheridan, "Photopolymer holographic recording material," Optik (Stuttgart) **112**, 449–463 (2001).
6. S. Blaya, L. Carretero, R. F. Madrigal, M. Ulibarrena, P. Acebal, and A. Fimia, "Photopolymerization model for holographic gratings formation in photopolymers," Appl. Phys. B **77**, 639–662 (2003).
7. M. R. Gleeson, J. V. Kelly, D. Sabol, C. E. Close, S. Liu, and J. T. Sheridan, "Modelling the photochemical effects present during holographic grating formation in photopolymer materials," J. Appl. Phys. **102**, 023108 (2007).
8. M. R. Gleeson, D. Sabol, S. Liu, C. E. Close, J. V. Kelly, and J. T. Sheridan, "Improvement of the spatial frequency response of photopolymer materials by modifying polymer chain length," J. Opt. Soc. Am. B **25**, 396–406 (2008).
9. M. R. Gleeson and J. T. Sheridan, "Non-local photopolymerization kinetics including multiple termination mechanisms and dark reactions: Part I. Modelling," J. Opt. Soc. Am. B **26**, 1736–1745 (2009).
10. M. R. Gleeson, S. Liu, R. R. McLeod, and J. T. Sheridan, "Non-local photo-polymerization kinetics including multiple termination mechanisms and dark reactions: Part II. Experimental validation," J. Opt. Soc. Am. B **26**, 1746–1754 (2009).
11. L. Dhar, A. Hale, H. E. Katz, M. L. Schilling, M. G. Schnoes, and F. C. Schilling, "Recording media that exhibit high dynamic range for digital holographic data storage," Opt. Lett. **24**, 487–489 (1999).
12. S. Schultz, E. Glytsis, and T. Gaylord, "Design, fabrication, and performance of preferential-order volume grating waveguide couplers," Appl. Opt. **39**, 1223–1232 (2000).
13. A. Sato, M. Scepanovic, and R. Kostuk, "Holographic edge-illuminated polymer Bragg gratings for dense wavelength division optical filters at 1550 nm," Appl. Opt. **42**, 778–784 (2003).
14. R. R. McLeod, A. J. Daiber, M. E. McDonald, T. L. Robertson, T. Slagle, S. L. Sochava, and L. Hesselink, "Microholographic multilayer optical disk data storage," Appl. Opt. **44**, 3197–3207 (2005).
15. F. Bruder and T. Faecke, "Materials in optical data storage," Int. J. Mater. Res. **101**, 199–215 (2010).
16. InPhase Technologies, Tapestry Media, www.inphase-technologies.com.
17. M. Straub, L. H. Nguyen, A. Fazlic, and M. Gu, "Complex-shaped 3-D microstructures and photonic crystals generated in a polysiloxane polymer by two-photon microstereolithography," Opt. Mater. **27**, 359–364 (2004).
18. J. Zhang, K. Kasala, A. Rewari, and K. Saravanamuttu, "Self-trapping of spatially and temporally incoherent white light in a photochemical medium," J. Am. Chem. Soc. **128**, 406–407 (2006).
19. G. H. Zhao and P. Mouroulis, "Diffusion-model of hologram formation in dry photopolymer materials," J. Mod. Opt. **41**, 1929–1939 (1994).
20. S. Piazzolla and B. K. Jenkins, "Holographic grating formation in photopolymers," Opt. Lett. **21**, 1075–1077 (1996).
21. V. L. Colvin, R. G. Larson, A. L. Harris, and M. L. Schilling, "Quantitative model of volume hologram formation in photopolymers," J. Appl. Phys. **81**, 5913–5923 (1997).
22. D. J. Lougnot, P. Jost, and L. Lavielle, "Polymers for holographic recording. VI. Some basic ideas for modelling the kinetics of the recording process," Pure Appl. Opt. **6**, 225–245 (1997).
23. I. Aubrecht, M. Miler, and I. Koudela, "Recording of holographic diffraction gratings in photopolymers: Theoretical modelling and real-time monitoring of grating growth," J. Mod. Opt. **45**, 1465–1477 (1998).
24. J. H. Kwon, H. C. Hwang, and K. C. Woo, "Analysis of temporal behavior of beams diffracted by volume gratings formed in photopolymers," J. Opt. Soc. Am. B **16**, 1651–1657 (1999).
25. J. T. Sheridan and J. R. Lawrence, "Nonlocal response diffusion model of holographic recording in photopolymer," J. Opt. Soc. Am. A **17**, 1108–1114 (2000).
26. C. Neipp, S. Gallego, M. Ortuno, A. Marquez, M. L. Alvarez, A. Belendez, and I. Pascual, "First-harmonic diffusion-based model applied to a polyvinyl-alcohol—acrylamide-based photopolymer," J. Opt. Soc. Am. B **20**, 2052–2060 (2003).
27. J. V. Kelly, M. R. Gleeson, C. E. Close, F. T. O'Neill, J. T. Sheridan, S. Gallego, and C. Neipp, "Temporal analysis of grating formation in photopolymer using the nonlocal polymerization-driven diffusion model," Opt. Express **13**, 6990–7004 (2005).
28. J. T. Sheridan, M. R. Gleeson, C. E. Close, and J. V. Kelly, "Optical response of photopolymer materials for holographic data storage applications," J. Nanosci. Nanotechnol. **7**, 232–242 (2007).
29. M. R. Gleeson and J. T. Sheridan, "A review of the modelling of free-radical photopolymerisation in the formation of holographic gratings," J. Opt. A, Pure Appl. Opt. **11**, 024008 (2009).
30. T. Trentler, J. Boyd, and V. Colvin, "Epoxy resin photopolymer composites for volume holography," Chem. Mater. **12**, 1431–1438 (2000).
31. M. R. Gleeson, S. Liu, S. O'Duill, and J. T. Sheridan, "Examination of the photoinitiation processes in photopolymer materials," J. Appl. Phys. **104**, 064917 (2008).
32. S. Liu, M. R. Gleeson, and J. T. Sheridan, "Analysis of the photoabsorptive behavior of two different photosensitizers in a photopolymer material," J. Opt. Soc. Am. B **26**, 528–536 (2009).
33. S. Liu, M. R. Gleeson, D. Sabol, and J. T. Sheridan, "Extended model of the photoinitiation mechanisms in photopolymer materials," J. Appl. Phys. **106**, 104911 (2009).
34. S. Liu, M. R. Gleeson, J. Guo, and J. T. Sheridan, "Optical characterization of photopolymers materials: Theoretical and experimental examination of primary radical generation," Appl. Phys. B **100**, 559–569 (2010).
35. L. Carretero, S. Blaya, R. Mallavia, R. F. Madrigal, A. Belendez, and A. Fimia, "Theoretical and experimental study of the bleaching of a dye in a film-polymerization process," Appl. Opt. **37**, 4496–4499 (1998).
36. S. Gallego, M. Ortuno, C. Neipp, A. Marquez, A. Belendez, I. Pascual, J. V. Kelly, and J. T. Sheridan, "Physical and effective optical thickness of holographic diffraction gratings recorded in photopolymers," Opt. Express **13**, 1939–1947 (2005).
37. G. Odian, *Principles of Polymerization* (Wiley, 1991).
38. A. Fimia, N. Lopez, F. Mateos, R. Sastre, J. Pineda, and F. Amatguerri, "Elimination of oxygen inhibition in photopolymer system used as holographic recording materials," J. Mod. Opt. **40**, 699–706 (1993).
39. M. R. Gleeson, J. V. Kelly, C. E. Close, F. T. O'Neill, and J. T. Sheridan, "Effects of absorption and inhibition during grating formation in photopolymer materials," J. Opt. Soc. Am. B **23**, 2079–2088 (2006).
40. F. T. O'Neill, J. R. Lawrence, and J. T. Sheridan, "Improvement of holographic recording material using aerosol solvent," J. Opt. A, Pure Appl. Opt. **3**, 20–25 (2001).
41. J. Crank, *The Mathematics of Diffusion*, 2nd ed. (Oxford Univ. Press, 1976).
42. H. Kogelnik, "Coupled wave theory for thick hologram gratings," Bell Syst. Tech. J. **48**, 2909–2945 (1969).